

The solar modulation of protons and anti-protons

Aslam, O. P. M.*

Centre for Space Research, North-West University, 2520 Potchefstroom, South Africa

E-mail: aslamklr2003@gmail.com

Driaan Bisschoff

Centre for Space Research, North-West University, 2520 Potchefstroom, South Africa

E-mail: driaanb@gmail.com

Marius S Potgieter

Centre for Space Research, North-West University, 2520 Potchefstroom, South Africa

E-mail: marinus.potgieter@nwu.ac.za

A comprehensive, three-dimensional drift model is used to study the solar modulation of cosmic ray protons and particularly of anti-protons. Spectra for protons and anti-protons from 10 MeV to 70 GeV are computed based on revisited local interstellar spectra for these particles. This is done for a complete solar cycle from 2006 to 2017, which includes the prolonged deep solar minimum period of 2006–2009 and the magnetic polarity reversal period of Oct 2012 to April 2014. The study highlights the modulation differences between these particles and addresses the level of particle drifts that is required to explain in detail the observed ant-proton to proton ratio, especially for the reversal period.

*36th International Cosmic Ray Conference -ICRC2019-
July 24th - August 1st, 2019
Madison, WI, U.S.A.*

*Speaker.

1. Introduction

The availability of proton spectra precisely measured by *PAMELA* during the unusual solar minimum of 2006–2009 [1], and *AMS-02* for the 2011–2017 period [2], will assist to study the heliospheric modulation of cosmic ray (CRs) protons in detail for the period 2006–2017. The modulation of CR particles over the unusual minimum period of 2006–2009, especially galactic protons, is studied in detail by [3,4]. All four major modulation mechanisms are important in the modulation of CRs, but their relative importance varies throughout the solar cycle [3]. It is generally accepted that gradient, curvature and heliospheric current sheet (HCS) drifts can dominate CR modulation during minimum phases of solar activity, and its modulation effects reduce for solar activity maximum phases, when modulation is mainly determined by large-scale disturbances in the solar wind, see [5-8] and [3,9,10]. The previous solar minimum of 2009 was special because then a record high intensity of protons was reported [1,3] at the end of 2009. Neutron monitors also reported record high counts (cosmicrays oulu.fi). Modulation studies for the period 2006–2009 conclude that all modulation process had played important roles during this unusual minimum period, especially particle drifts, but that diffusion was relatively dominant; see [3,4,12,13] and reviews [5,11].

Drift modulation models predict that positively charged CRs drift inward to the inner heliosphere mainly along the equator and outward via the polar regions during the negative polarity phase ($A < 0$) so that they encounter the changing wavy HCS during their entry (as happened from 2001–2012), and that the drift direction reverses when the Sun's magnetic polarity is completely switched. For negatively charged CRs (anti-protons, electrons) the drift velocity is oppositely directed [12,13]. We are interested in how solar modulation varies from one activity minimum to the next, and how particle drift effects vary from one polarity phase to another. It is our expectation that the available CR spectra from *PAMELA* and *AMS-02* from 2006–2017 will assist modeling studies of both protons and anti-protons over roughly a complete solar cycle. The 690 days, 850 days and 3-year averaged *PAMELA* observations [14-16], 4-year averaged *AMS-02* observations [17], for anti-proton spectrum and anti-proton to proton ratio, and the anti-proton modeling results reported by [18] using a two-dimensional drift dominated model, will be most useful to test and validate anti-proton modeling results, especially the temporal variation in the anti-proton to proton ratio before and after the polarity reversal. This is in addition to what was observed and modelled for the variation of the positron to electron ratio reported by [19,20].

We present preliminary results of a proton and anti-proton modeling study, a continuation of previous detailed studies using a comprehensive three-dimensional (3D) modulation model including drifts as applied to galactic protons [3,4], electrons [12] and positrons [13] using *PAMELA* observations [1,21-23] during quiet heliospheric conditions (2006–2009). We consider protons from July 2006–May 2017 for which solar rotation averaged *PAMELA* spectra over an energy range of ~ 80 MeV to 50 GeV are available up to Dec 2009 [1] and Bartel rotation averaged *AMS-02* spectra over an energy range of ~ 1 GeV to 50 GeV from May 2011–May 2017 [2]. Because drift patterns differ for protons and anti-protons during $A < 0$ and $A > 0$ magnetic polarity phases, the anti-proton to proton ratio computations will contribute to understand how differently they get modulated during these polarity cycles, and how the major diffusion coefficients as well as drift effects change with time from one minimum activity phase to the next, through a full polarity reversal period.

2. Very Local Interstellar Spectra for protons and anti-protons

A galactic spectrum for protons and for anti-protons, more specifically a very local interstellar spectrum (LIS) has to be specified in the numerical modulation model to be used as an initial input spectrum, which is then modulated throughout the heliosphere. This is done at the modulation boundary of the heliosphere (heliopause) specified at 122 au. The proton LIS and the initial anti-proton LIS are computed with the GALPROP code, but we modify this anti-proton LIS based on our study using the *PAMELA* and *AMS-02* observations[14-17]; see examples and references in [24]. Figure 1 illustrates the very LIS for protons and the modified very LIS for anti-protons as used in our modulation modeling reported below.

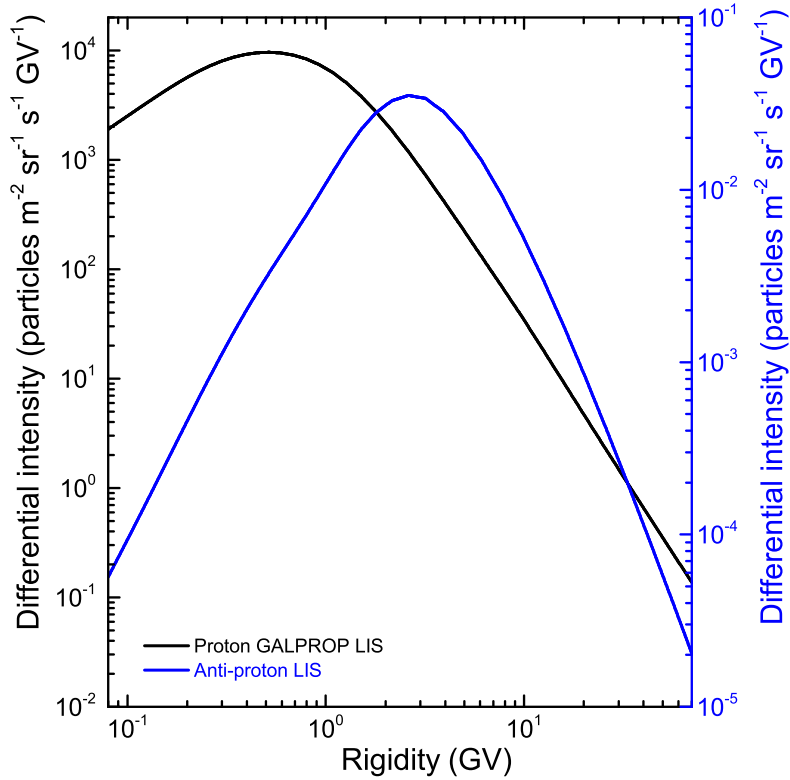


Figure 1: LIS for galactic protons (black line) computed with GALPROP and a modified LIS for anti-protons (blue line); black axis values correspond to the proton LIS; blue axis to the anti-proton LIS.

We begin with a GALPROP computed LIS for protons to reproduce the modulated *PAMELA* observations from 2006–2009. This proton LIS is used then to reproduce the *AMS-02* proton observations from May 2011–May 2017. Next, the same modulation parameter set as for protons is used to compute corresponding anti-proton spectra for the whole period throughout the heliosphere, with respect to the modified anti-proton LIS.

3. The numerical modulation model

A comprehensive 3D modulation model based on the numerical solution of the Parker transport

equation [TPE, 25] is used to compute the differential intensity of CR protons and anti-protons, over an energy range of 10 MeV–70 GeV, at increasing radial distances from the Earth (1 au) up to the heliopause (122 au). This TPE is described as:

$$\frac{\partial f}{\partial t} = -\vec{V}_{sw} \cdot \nabla f - \langle \vec{v}_D \rangle \cdot \nabla f + \nabla \cdot (\mathbf{K}_s \cdot \nabla f) + \frac{1}{3} (\nabla \cdot \vec{V}_{sw}) \frac{\partial f}{\partial \ln P}, \quad (3.1)$$

where $f(\vec{r}, P, t)$ is the CR distribution function, P is rigidity, t is time, and \vec{r} is the vector position in 3D, with the three coordinates r , θ , and ϕ specified in a heliocentric spherical coordinate system where the equatorial plane is at a polar angle of $\theta = 90^\circ$. The four terms shown on the right-hand side of Equation (3.1) represent the four major physical processes which CR particles undergo when they enter and travel through the heliosphere up to the Earth.

The model and modulation parameters are described in detail by [3,4,12,13]. We solve the TPE for selected intervals (minimum of one solar or Bartel rotation, see [13]) by using the averaged values of the HCS tilt angle α , the HMF magnitude B at the Earth, and by adjusting the three diffusion and one drift coefficients. The very LIS for protons and anti-protons are used as discussed above (see Figure 1) in an assumed heliosphere with the heliopause at 122 au. The 3D model also includes a heliosheath with a varying width as solar activity changes [4,13].

4. Comparison of modeling results with observations

We consider seven data sets of *PAMELA* proton observations, each 27-day averaged, over an energy range of ~ 80 MeV–50 GeV, from July 2006–Dec 2009. We additionally use *AMS-02* proton observations, which is averaged over Bartel rotations, over an energy range of ~ 1 –50 GeV, from May 2011–May 2017. For the latter, we consider only two sets for each year, one corresponding to the middle of a year and the other one to the end of this particular year.

First, we start with the proton observations of Nov 13–Dec 04, 2006 and reproduce the *PAMELA* spectrum as shown in Figure 2(a). The averaged HMF magnitude at Earth is $B = 4.95$ nT and the tilt angle $\alpha = 16.8^\circ$ during this period. How B and α are calculated for each period, and the procedure of parameter selection and their values are explained in detail by [13]. Similarly, we reproduce all *PAMELA* spectra from 2006–2009. Figure 2(b) shows only the computed spectra for Dec 06, 2009–Jan 01, 2010. During this period $\alpha = 9.5^\circ$ and $B = 3.91$ nT. Changing only these two values with time cannot reproduce all the observed spectra, so we need to change in addition the diffusion coefficients [3]. For the 2006–2009 minimum period, we keep the drift coefficient at its maximum level [13]. Based on our understanding of proton and anti-proton modulation, we use the same parameter set to compute the anti-proton spectra.

Figures 2(c) and 2(d) show the simulated *AMS-02* proton spectra for the periods May 20–Jun 10, 2011 (rotation 2426; start of the observations) and April 13–May 09, 2017 (rotation 2506; end of the published *AMS-02* observations). The averaged $B = 4.84$ nT, and $\alpha = 35.38^\circ$ for the 2426 rotation, with $B = 5.74$ nT and $\alpha = 22.49^\circ$ for the 2506 rotation. Similar to rotations 2426 and 2506, we reproduce all the *AMS-02* proton spectra. In addition to changing B and α for each period, we need to adjust the drift coefficient from 0 (for uncertain polarity periods) to 0.90, and also the diffusion coefficients to reproduce these observations. Then we use the same parameter set to produce the anti-proton modeling results, shown only corresponding results for the beginning and ending of the proton data sets of both *PAMELA* and *AMS-02* observations.

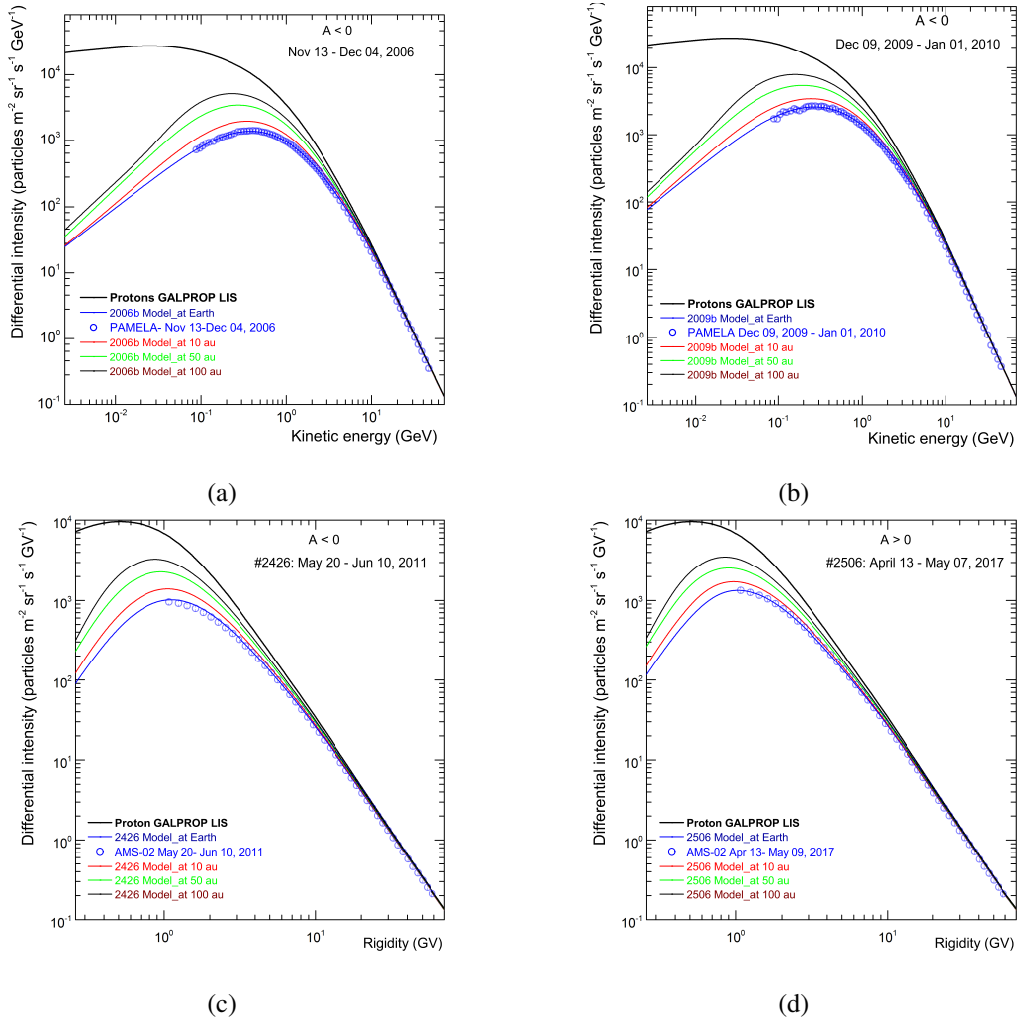


Figure 2: Computed proton spectra for (a) Nov 13–Dec 06, 2006 (b) Dec 06, 2009–Jan 01, 2010 (c) May 20–June 10, 2011, and (d) April 13–May 09, 2017, for increasing radial distances, at Earth (blue), 10 au (red), 50 au (green), and 100 au (black). Black thick line is the GALPROP LIS specified at 122 au, the distance to the heliopause. Blue circles are *PAMELA* or *AMS-02* proton observations for time periods as indicated. In (a) and (b) the plot is for differential intensity, particles m⁻² sr⁻¹ s⁻¹ GeV⁻¹, against kinetic energy, but (c) and (d) are for particles m⁻² sr⁻¹ s⁻¹ GV⁻¹ against rigidity (GV).

Figures 3(a) and 3(b) show the computed modulated spectra of protons and anti-protons at Earth (1 au), with respect to their respective LISs at 122 au, as a function of rigidity for the periods indicated in the figure caption.

In order to check and confirm the general shape of the anti-proton spectra and the anti-proton to proton ratio, the *AMS-02* anti-proton observations over the average period May 19, 2011–May 26, 2015 [17] is compared with our computed anti-proton spectra in Figure 4(a) and with the corresponding anti-proton to proton ratio in Figure 4(b).

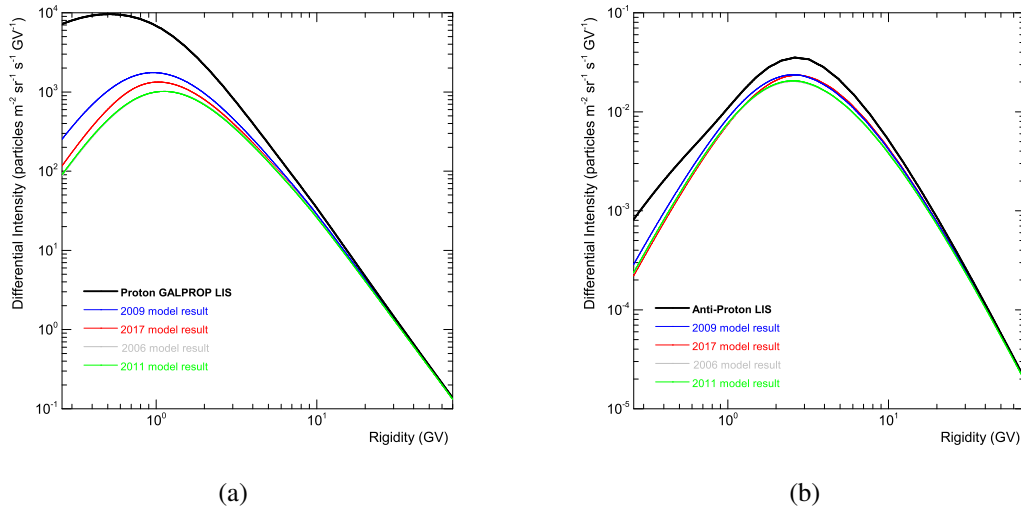


Figure 3: Computed spectra for (a) protons and (b) anti-protons at Earth, for Nov 13–Dec 04, 2006 (gray line), Dec 06, 2009–Jan 01, 2010 (blue line), May 20–June 10, 2011 (green line) and April 13–May 09, 2017 (red line). Black solid line in (a) is the GALPROP proton LIS; in (b) it is our modified anti-proton LIS. First three periods belong to the $A < 0$ phase but the last one belongs to the $A > 0$ phase.

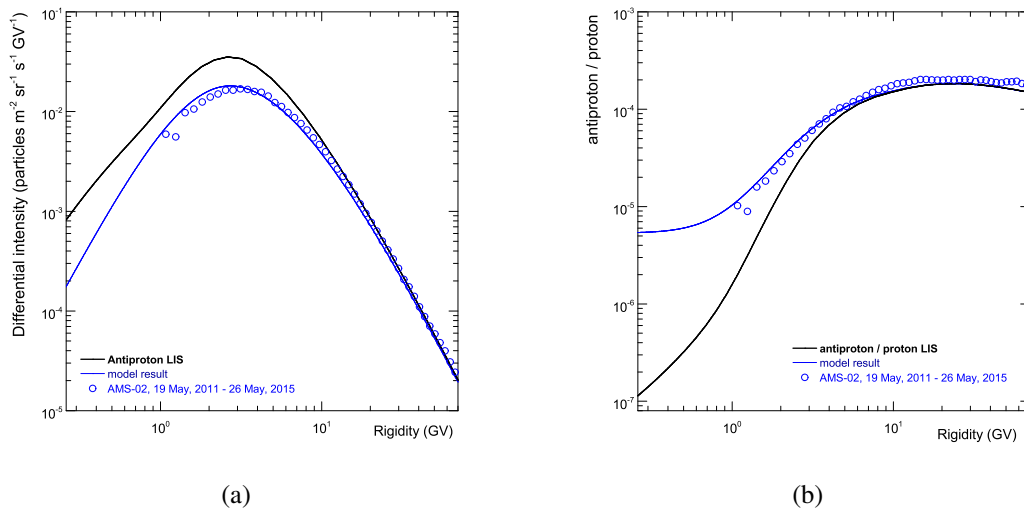


Figure 4: Computed anti-proton spectra in (a) as a function of rigidity for May 19, 2011–May 26, 2015 and in (b) the corresponding anti-proton to proton ratio for the same period. Black thick line in (a) is our anti-proton LIS, and in (b) it is the ratio between this anti-proton LIS and the GALPROP proton LIS. Blue circles represent *AMS-02* observations in (a) and in (b).

4.1 Anti-proton to proton ratio

After reproducing the *AMS-02* proton and corresponding anti-proton spectra, we calculate the subsequent anti-proton to proton ratio as a function of time for kinetic energy of 1.0–1.5 GeV, as an illustrative example. Figure 5 shows how this ratio varies from 2011–2017. It increases gradually from 2011 to reach a maximum in Nov–Dec 2013, then decreases back to a minimum in Jan 2017. In order to reproduce the *AMS-02* ratio, and apart from varying the diffusion coefficients, we have to keep the drift coefficient at a minimum level [13] for the solar maximum period, and then have to increase it gradually to a maximum value as solar activity decreases to a minimum. The drift coefficient is at its maximum value during the 2006–2009 minimum period to decrease gradually up to its lowest value for the 2012–2014 reversal period, then increasing gradually back to a maximum value in Dec 2016. See also [19, 20, 26] on how the positron to electron ratio varies during this same period.

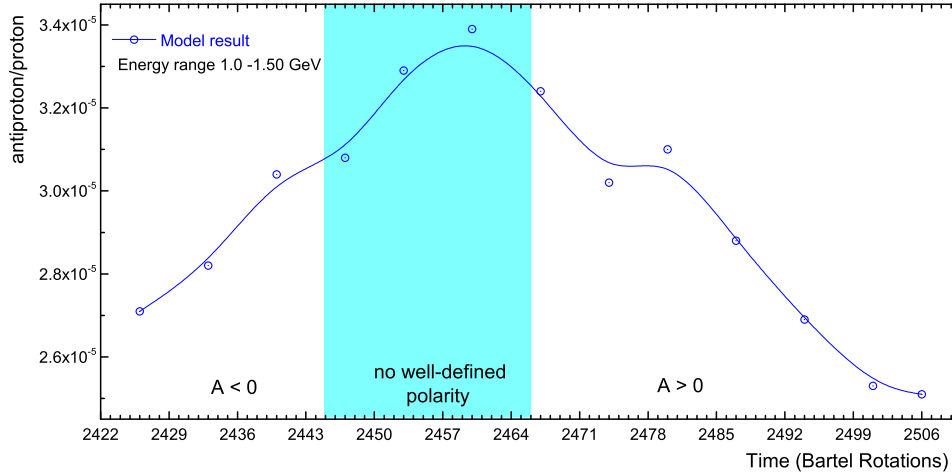


Figure 5: Computed anti-proton to proton ratio (solid blue line) in comparison with *AMS-02* observations for Bartel rotations, 2426–2506, the time period May, 2011–May, 2017, for kinetic energy 1.0–1.5 GeV. HMF reversal period during which no well-defined polarity was exhibited is indicated, with $A < 0$ before this reversal and $A > 0$ afterwards.

5. Summary and Conclusion

The overall objective of this preliminary study is the reconstruction of the combined *PAMELA* and *AMS-02* proton observations from July 2006 to May 2017, and then apply the model to produce corresponding anti-proton spectra, and in particular to compute the anti-proton to proton ratio before and after the HMF polarity reversal as shown in Figure 5. That is accomplished by using a 3D drift modulation model, changing the averaged HCS tilt angle and the HMF magnitude at the Earth with time, which we consider as very good proxies for solar activity. Changing their values directly affects the values of the diffusion and drift coefficients. However, in order to reproduce and explain the observed anti-proton to proton ratio, it is necessary to adjust additionally the diffusion

coefficients and very specifically the drift coefficient gradually over time, with the latter becoming zero during the HMF polarity reversal period.

We thank the GALPROP developers for access to and use of the GALPROP WebRun service. We acknowledge the use of HCS tilt angle data from the Wilcox Solar Observatory, <http://wso.stanford.edu>, and HMF data from the NASA OMNIWEB, <http://omniweb.gsfc.nasa.gov>.

References

- [1] O. Adriani, G. C. Barbarino, G. A. Bazilevskaya, et al. *Astrophys. J.* 765, 91, 2013.
- [2] M. Aguilar, M., L. Ali Cavazonza, G. Ambrosi, et al. *Phys. Rev. Lett.* 121, 051101, 2018.
- [3] M. S. Potgieter, E. E. Vos, M. Boezio, et al. *Solar Phys.* 289, 391, 2014.
- [4] E. E. Vos, M. S. Potgieter. *Astrophys. J.* 815, 119, 2015.
- [5] M. S. Potgieter. *Living Rev. in Solar Phys.* 10, 3, 2013.
- [6] B. Heber. *Space Sci. Rev.* 176, 265, 2013.
- [7] B. Heber, M. S. Potgieter. *Space Sci. Rev.* 127, 117, 2006.
- [8] R. B. McKibben, J. J. Connel, C. Lopate, et al. *Space Sci. Rev.* 72, 367, 1995.
- [9] F. B. McDonald, L. Nand, R. E. McGuire. *J. Geophys. Res.* 98, 1243, 1993.
- [10] O. P. M. Aslam, Badruddin. *Solar Phys.* 279, 269, 2012.
- [11] M. S. Potgieter. *Adv. Space Res.* 60, 848, 2017.
- [12] M. S. Potgieter, E. E. Vos, R. Munini, et al. *Astrophys. J.* 810, 141, 2015.
- [13] O.P. M. Aslam, D. Bisschoff, M. S. Potgieter, et al. *Astrophys. J.* 873, 70, 2019.
- [14] O. Adriani, G. C. Barbarino, G. A. Bazilevskaya, et al. *Phys. Rev. Lett.* 102, 051101, 2009.
- [15] O. Adriani, G. C. Barbarino, G. A. Bazilevskaya, et al. *Phys. Rev. Lett.* 105, 121101, 2010.
- [16] O. Adriani, G. A. Bazilevskaya, G. C. Barbarino, et al. *JETP Lett.* 96, 621, 2013.
- [17] M. Aguilar, M., L. Ali Cavazonza, G. Ambrosi, et al. *Phys. Rev. Lett.* 117, 091103, 2016.
- [18] W. R. Webber, M. S. Potgieter. *Astrophys. J.* 344, 779, 1989.
- [19] O. Adriani, G. C. Barbarino, G. A. Bazilevskaya, et al. *Phys. Rev. Lett.* 116, 241105, 2016.
- [20] M. Aguilar, M., L. Ali Cavazonza, G. Ambrosi, et al. *Phys. Rev. Lett.* 121, 051102, 2018.
- [21] O. Adriani, G. C. Barbarino, G. A. Bazilevskaya, et al. *Astrophys. J.* 810, 142, 2015.
- [22] O. Adriani, G. C. Barbarino, G. A. Bazilevskaya, et al. *Phys. Rev. Lett.* 111, 081102, 2013.
- [23] R. Munini, V. di Felice, M. Boezio, et al. *Proc. Sci.* (35th ICRC) 301, 012, 2017.
- [24] D. Bisschoff, M. S. Potgieter, O. P. M. Aslam. *Astrophys. J.* 878, 59, 2019.
- [25] E. N. Parker. *Astrophys. J.* 128, 664, 1958.
- [26] O.P. M. Aslam, D. Bisschoff, M. S. Potgieter. *Proc. Sci.* (ICRC2019), 1053, 2019.